THE JOURNAL OF PHYSICAL CHEMISTRY B

Article

pubs.acs.org/JPCB

Substituent Effect on the Structural Behavior of Modified Cyclodextrin: A Molecular Dynamics Study on Methylated β-CDs

Wan-Sheung Li, San-Chi Wang, Tsong-Song Hwang, and Ito Chao*

Institute of Chemistry, Academia Sinica, Taipei, Taiwan, 11529

Supporting Information

ABSTRACT: A series of methylated and non-methylated β-cyclodextrin (β-CD) structures in three macrocyclic configurations (*a*–*c*) were studied with molecular dynamics (MD) simulations to elucidate the dynamic behavior of the different CD structures using a continuum water model with the AMBER* force field. A set of parameters were defined to describe the geometric dimensions of the CD, such as its cavity shape, the upper and lower rim sizes, and the tilting of each of the glucose rings. Correlation analyses between the different parameters were carried out, and they have provided insights into the different dynamic behaviors for the different CD structures. Detailed analyses on the crystal structures of the different methylated and non-methylated β-CD complexes were also carried out using the defined parameters. Correlation of parameters from crystal structures and MD simulations has allowed us to identify the effect that crystal packing/guest inclusion has on the CD geometries. The overall analysis approach can be a useful tool for other related macrocyclic structures, such as modified α-, β-CDs or even calixarenes.

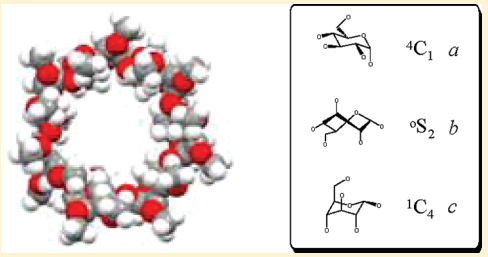

INTRODUCTION

Cyclodextrins (CDs) with their well-defined torus-like hydrophobic cavities combined with their hydrophilic hydroxyl rims have made them attractive candidates as hosts to a wide range of molecules and ions. Since the emergence of their inclusion properties, vast amounts of research have accumulated ranging from the role as chiral separators to possible enzyme models. Their functions are further enhanced by the possibility of attaching functional groups onto the periphery of the CD cavities. A number of mechanisms[1−3] are used to explain the inclusion process, from the rigid lock-and-key principles[1] to the flexible induced-fit mechanism.[2]

The general view of rigidity in α- and β-CDs is under increasing scrutiny, with experimental evidence such as ^{1}H NMR[4] and X-ray crystal structures challenging the conventional view.[5,6] As an enzyme mimic, structural flexibility to allow induced fit is desirable in the macrocyclic host. The development of a new form of cyclooligosaccharide hosts made from nonglucose sugar units has been reported.[7−9] Greater macrocycle flexibility was observed in α-cycloaltrin (with six α-D-altropyranose rings)[7] and monoaltro-β-CD,[8] where the hydroxyl group at C-2 and C-3 of the altropyranose ring is at an axial position instead of the equatorial position in the glucose unit. In these compounds, the altropyranose ring is observed to undergo dynamic $^4C_1 \rightleftharpoons {}^0S_2 \rightleftharpoons {}^1C_4$ equilibrium at room temperature, resulting in different macrocyclic shapes. The monoaltro-β-CD can also undergo distinct conformational change upon guest inclusion with adamantanecarboxylate, with the conformation of the altropyranose ring changed from the predominant $^1C_4$ to the $^0S_2$ form, creating a bigger cavity volume to accommodate the guest. Other forms of ring skeleton modification on CDs with nonsugar units have also been reported, where substitution with an aromatic spacer,[10a,b] with one or two triazole units,[10c,d] and with a hexa-2,5-diyne-1,6-dioxy unit[10c] was used. Thioether substitution[10g] and a β-1,4 rather than α-1,4 glycosidic linkage[10h] have been reported. Replacement of a glycosidic linkage with a disulfide unit was also used to extend the linkage between the glucose rings.[10e,f]

The only direct experimental evidence for the two common CDs, α- and β-CD, pointing to the dynamic flexibility of the macrocycle as observed in the altropyranose substituted cyclooligosaccharides, is from a sporadic list of X-ray crystal structures of per-substituted β-CDs.[6a,e,f] In unsubstituted β-CD, the cyclic oligosaccharide is linked by seven α-(1,4) glucose units all in the $^4C_1$ chair configuration (termed form *a* in

Scheme 1. Three Different Forms of Cyclodextrin Structures (*a*–*c*)[a]

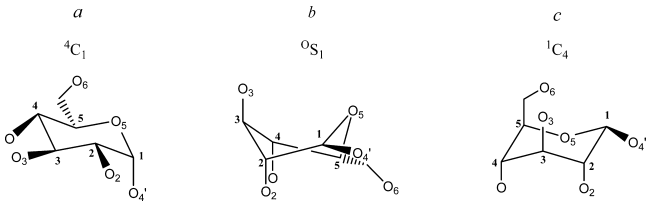

[a]In *a*, all the rings are in the $^4C_1$ conformation, and in *b* and *c*, one of the glucose rings is in a $^0S_2$ and $^1C_4$ conformation, respectively. Only one glucose ring is shown.

Received: August 19, 2011
Revised: January 20, 2012
Published: February 13, 2012

   dx.doi.org/10.1021/jp207985q | *J. Phys. Chem. B* 2012, 116, 3477–3489

Scheme 1). Substitution can take place in the three hydroxyl sites, O_2, O_3, and O_6, as shown in Scheme 2. Steric

Scheme 2. Unmethylated β-CD (0) and Three Methylated β-CDs (1−3) under Investigation

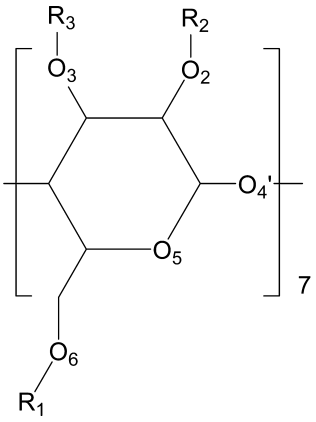

	R_1	R_2	R_3
0	H	H	H
1	CH_3	H	H
2	CH_3	CH_3	H
3	CH_3	CH_3	CH_3

overcrowding by bulky substituent groups (R = *tert*-butyldimethylsilyl,[11] acetyl,[12] and propanol[12]) can induce conformational change of the CD macrocycle to *b* or *c* forms, where one of the glucose units flipped to a $^1C_4$ or $^0S_2$ configuration, respectively (Scheme 1). Even with the simplest modification, methylation on β-CD can yield a macrocyclic conformation in three different forms (*a*−*c*). The 2,6-dimethyl-substituted α- and β-CDs and the 2,3,6-trimethyl-substituted α-CDs yield crystal structures with macrocyclic conformation *a*.[5,6] However, the fully methylated β-CD (TM-β-CD **3**; Scheme 2) can adopt a macrocyclic conformation with one of the glucose units in three different conformations. Guest-induced conformational change in TM-β-CD to **3b** with one $^0S_2$-twist boat glucose unit was observed in the crystal structure of TM-β-CD•*m*-iodophenol complex.[6a] The cyclic CD structure with a fully inverted glucose ring to the $^1C_4$ chair conformation (**3c**) was crystallized from hot water in the monohydrate TM-β-CD.[6e] It seems that, free from the geometric restraints imposed by the intramolecular $O_2\cdots O_3'$ hydrogen bonds, the fully methylated CD can adopt unusual macrocyclic conformations.

Since the emergence of CDs in host−guest complexation, a vast amount of data concerning their inclusion process have been accumulated. However, there remains a lack of complete understanding toward how selectivity is achieved. A general perception is that the mechanism of molecular recognition is different for different CD•guest systems. The main barrier for this lack of understanding is that CD hosts are not rigid and molecular recognition is not confined to its molecular cavity but also at the peripheries. Systematic crystallographic studies can provide valuable insight into the intermolecular interactions involved in molecular recognition, especially when crystal-packing effects do not appear to unduly influence those interactions. However, these structures are static and systematic analysis on their structural dynamics is limited to the structures that are available. Geometric complementarity, or spatial fit between host and guest, is one of the first requirements of molecular recognition by CDs. However, molecular selectivity can also be controlled by the induced-fit ability in CD which is recognized to be an essential mechanism to the success of CD•guest complexation. Up to now, understanding toward the structural flexibility of CD and their analogues has been limited. If we want to achieve fine control over complexation in CD•guest systems, a systematic approach is required to study their dynamic flexibility.

In this paper, we used β-CD and its methyl derivatives as starting models in our aim to gain insights into the structural dynamics of this type of host system with computational techniques. Three different macrocyclic conformations (*a*, *b*, and *c*) were examined for β-CD (**0**), the mono-6 (Me-β-CD **1**),

Scheme 3. Definitions of Parameters[a]

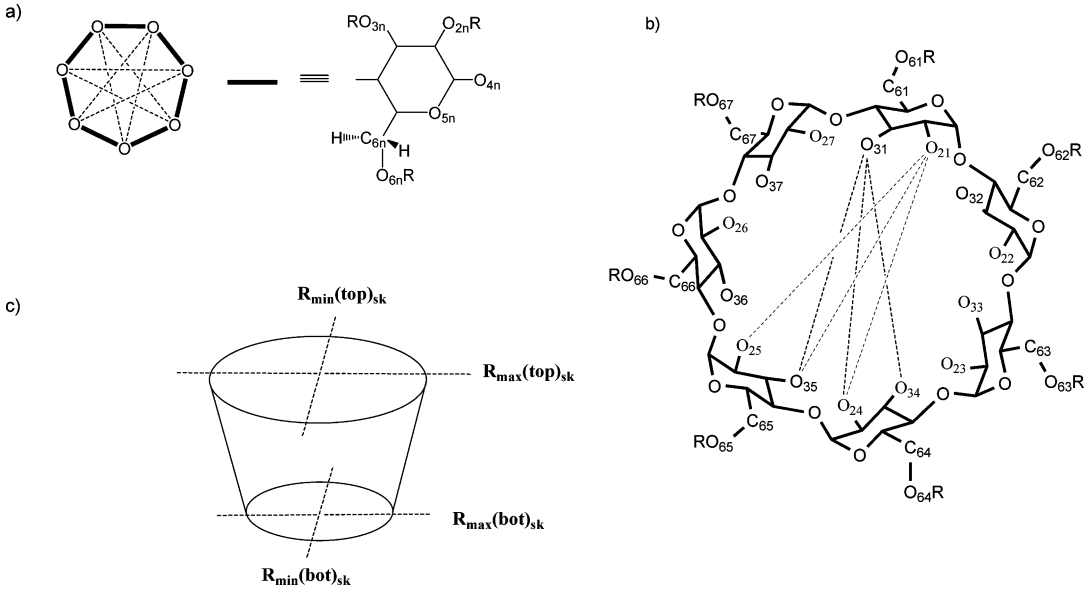

[a](a) The dotted lines show the seven pairs of glycosidic O···O distances, and the difference between the longest and the shortest of these distances gives $\Delta R_{l\text{-}s}$. (b) Labels for the O_{2n}, O_{3n}, and C_{6n} atoms used in the discussion for measuring the skeletal rim parameters. A set of three distances measured for O_{21} and O_{31} in glucose 1 is shown in dotted lines (see discussion). They are used for measuring $R_{max}(top)_{sk}$ and $R_{min}(top)_{sk}$; for the bottom rim, C_{6n} at opposite groups are measured (see text). (c) A scheme showing the *skeletal* rim parameters.

dx.doi.org/10.1021/jp207985q | J. Phys. Chem. B 2012, 116, 3477−3489

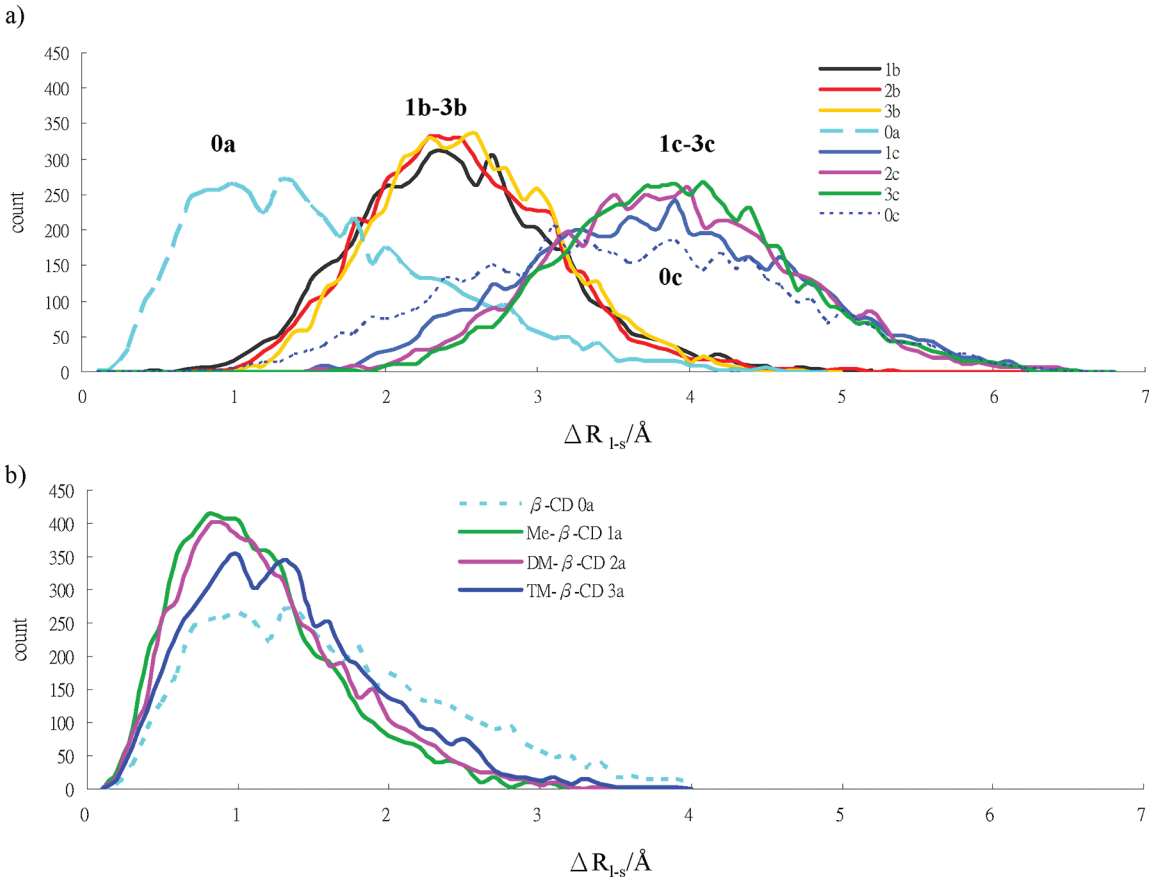

Figure 1. Population analyses of the sampled structures obtained from MD with $\Delta R_{l\text{-}s}$ of (a) **0a**, **1b**−**3b**, and **0c**−**3c** and (b) **0a**−**3a**.

di-2,6 (DM-β-CD **2**), and tri-2,3,6 methyl substituted β-CDs (TM-β-CD **3**), using molecular dynamics in a continuum water model with the AMBER* force field. Apart from identifying the different structural characteristics for the different compounds, their structural dynamics are compared in terms of cavity shape and size, ring tilting, and variation of the upper and lower rim openings of the macrocycles. Fundamental insights into the dynamic motion of the CD structures can be obtained by using simple correlation analysis between the various geometric parameters we have defined in this paper. Analyses were also preformed on solid state structures of β-CD and methylated β-CD complexes, and they showed the CD cavity is fairly flexible, changing its shape to adopt the different sizes and shapes of the guest molecules.

COMPUTATION METHODS

All stochastic molecular dynamics simulations were carried out using MacroModel V 6.5 and V 9.0[13] with the all atom AMBER* force field[14] in a continuum GB/SA model[15] for water. Constant dielectric treatment was used to estimate electrostatic interactions. A 200 ps equilibration step with a 1.5 fs time step was followed by a 5000 ps MD run with a 1.5 fs time step at 300 K.[16] Structures were sampled at a regular interval of 1 ps during the simulations. The starting structures of the ordered $^4C_1$ models of β-CD (**0a**−**3a**) were taken from a heptakis(2,6-di-*O*-methyl)-β-CD•*p*-nitrophenol complex (CSD code: DEZMIE10), with methyl groups on the O_2 sites substituted with H-atoms for **1a**, and addition of methyl groups on the O_3 sites for **3a**. The disordered $^0S_2$ (**0b**−**3b**) and $^1C_4$ (**0c**−**3c**) models were built from the heptakis(2,3,6-tri-*O*-methyl)-β-CD•m-iodophenol (CSD code: GELKEN10) and the monohydrate TM-β-CD (CSD code: HEZWAK01) complexes, respectively. To determine the relationship between two structural properties (x and y), Pearson correlation was used to calculate the correlation coefficient (1).[17]

$$r = \frac{n(\sum xy) - (\sum x)(\sum y)}{\sqrt{[n\sum x^2 - (\sum x)^2][n\sum y^2 - (\sum y)^2]}} \quad (1)$$

In the Results and Discussion, 5000 ps MD simulation results were used. The calculated correlation coefficients with values greater than 0.5 are considered moderately significant and correlation analyses using a smaller time frame at every 1000 ps showed consistent trends with the overall correlation coefficients calculated for 5000 ps (see Tables S1−S10, Supporting Information). This gives a good indication that the correlation between the various parameters is not a random observation. Simulations using 20 ns also showed consistent correlations of the various parameters that were observed in the 5000 ps MD simulations (Tables S11−13, Supporting Information); with the exception of **2b**, in which one of the glucose rings was flipped upside down at ∼9500 ps in the simulation (see Table S12, Supporting Information).

The CD torsion angles are translated to scalar $^3J_{CH}$ coupling constants using the Karplus-type relationship[18] in eq 2, where κ is the torsion angle ψ (C_1−O_4'−C_4'−H_4') or φ (H_1−C_1−O_4'−C_4').

$$^3J_{COCH} = 7.49\cos^2\kappa - 0.96\cos\kappa + 0.15 \quad (2)$$

dx.doi.org/10.1021/jp207985q | J. Phys. Chem. B 2012, 116, 3477−3489

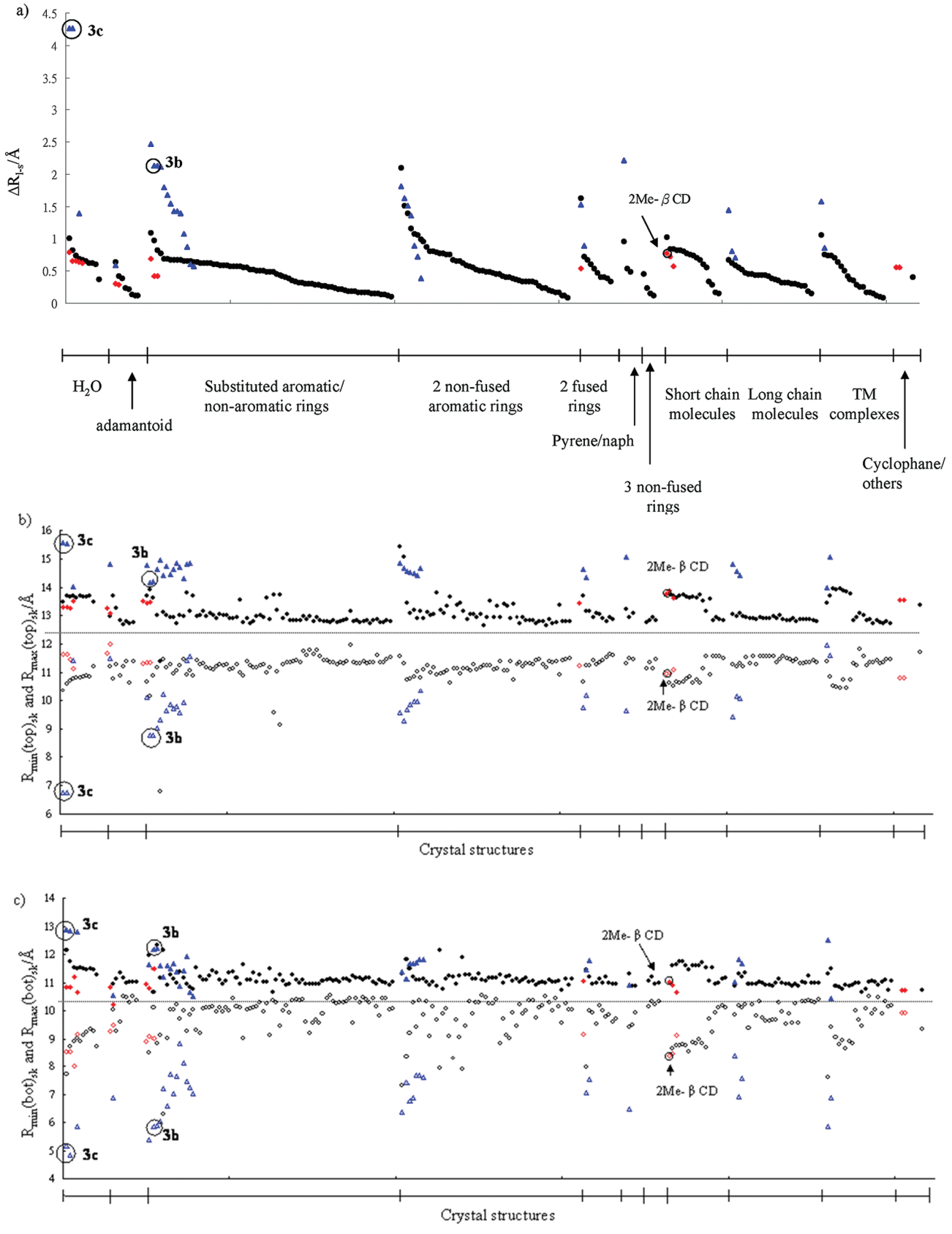

Figure 2. Analyses of crystal structures of 0a (●), **2a** (◆), and **3a** (▲); each data point represents one CD structure. The unusual 2-methylated *β*-CD (2Me-*β*CD) and the crystal structures with **3b** and **3c** conformations are also measured (circled in the figures). The values are shown according to the guest types in the complexes, and for clarity, they are shown in descending order of $\Delta R_{l\text{-}s}$. (a) Calculated $\Delta R_{l\text{-}s}$, (b) $R_{min}(top)_{sk}$ (open shapes) and $R_{max}(top)_{sk}$ (solid shapes), and (c) $R_{min}(bot)_{sk}$ (open shapes) and $R_{max}(bot)_{sk}$ (solid shapes).

dx.doi.org/10.1021/jp207985q | *J. Phys. Chem. B* 2012, 116, 3477−3489

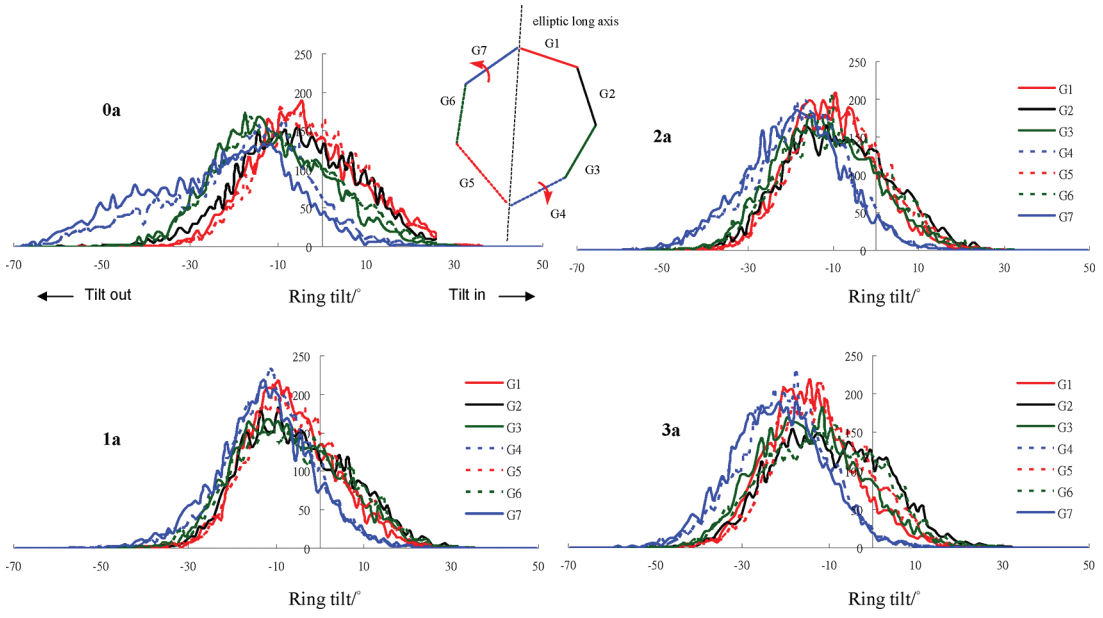

Figure 3. Population analyses of the tilting of the seven glucose rings (in deg) of **0a**−**3a** obtained from sampled structures during 5000 ps MD simulations. The red arrows indicate that G4 and G7 have a higher tendency to tilt out with respect to the glycosidic mean plane.

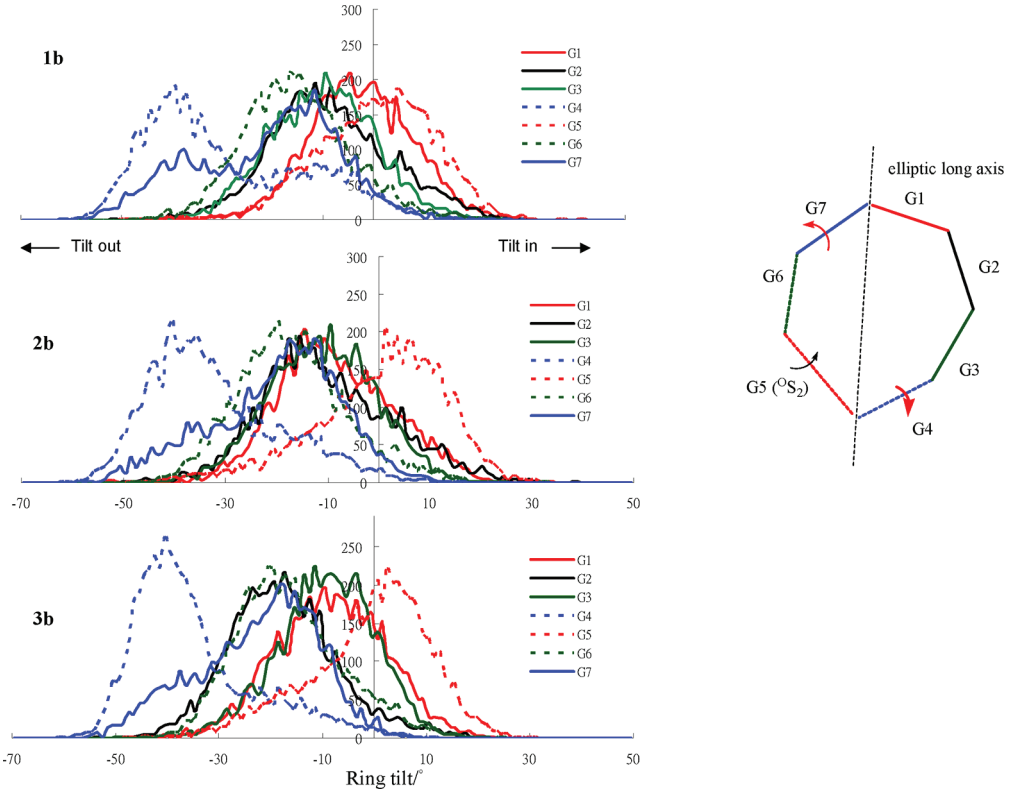

Figure 4. Population analyses of the tilting of the seven glucose rings (in deg) of **1b**−**3b** obtained from sampled structures during 5000 ps MD simulations. The $^{0}S_{2}$ glucose ring is labeled G5. The red and black arrows indicate rings have a large number of sampled structures tilted out and in, respectively.

RESULTS AND DISCUSSION

1. Stability of the Different CD Configurations. Studies have shown that under room temperature conditions α-cycloaltrin and monoaltro-β-CD can undergo conformational change with the altropyranose ring in dynamic equilibrium between $^{4}C_{1}$, $^{0}S_{2}$, and $^{1}C_{4}$ configurations. Macrocyclic conformational change upon guest inclusion was also observed in the monoaltro-β-CD•adamantanecarboxylate complex, from the predominant $^{1}C_{4}$ form in the free host to the $^{0}S_{2}$ form in the complex. As far as we acknowledge, there is no experimental evidence indicating the presence of this type of dynamic process for the parent β-CD, both in solution and in the solid state. Our simulations of β-CD in macrocyclic conformations *a*−*c* predict that for β-CD to coexist in the three

dx.doi.org/10.1021/jp207985q | J. Phys. Chem. B 2012, 116, 3477−3489

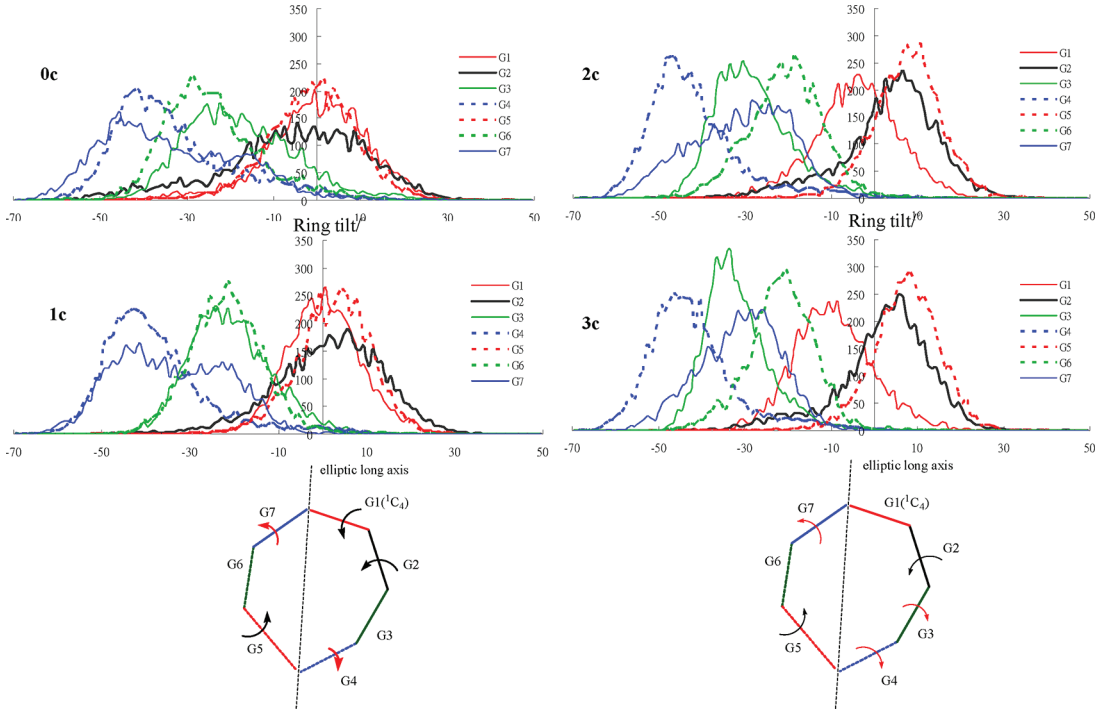

Figure 5. Population analyses of the tilting of the seven glucose rings (in deg) of **0c**−**3c** obtained from sampled structures during 5000 ps MD simulations. The $^1C_4$ glucose ring is labeled G1. The red and black arrows indicate that the glucose ring is tilted out and in, respectively.

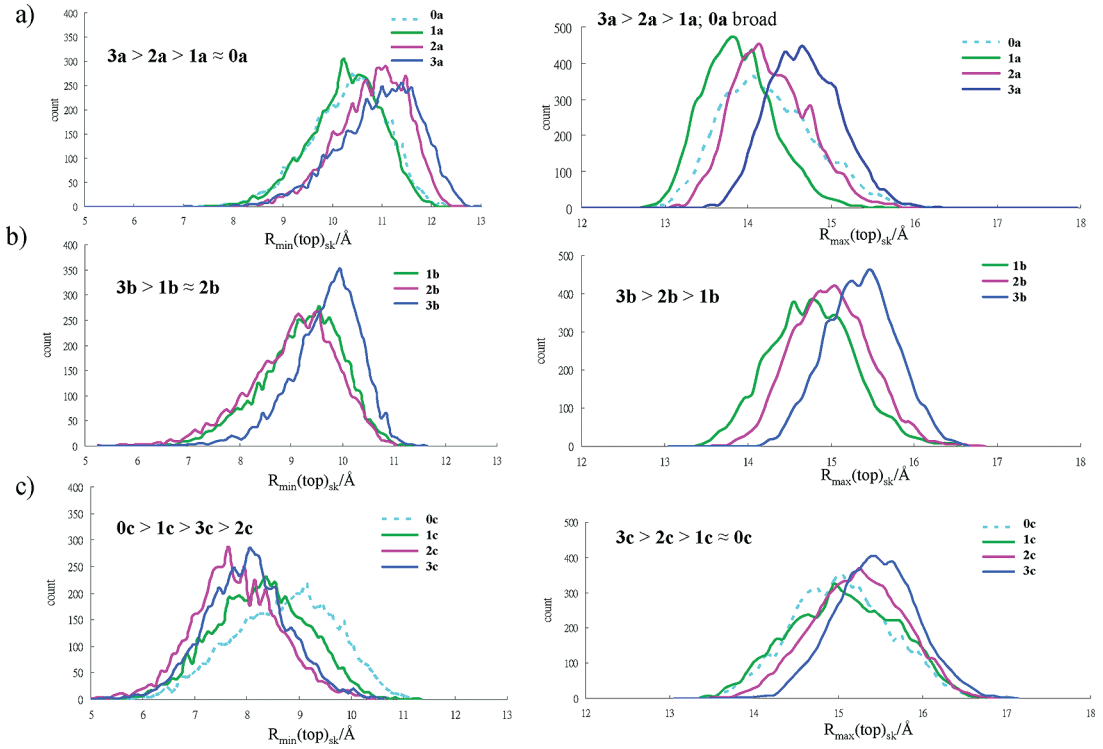

Figure 6. $R_{min}(top)_{sk}$ and $R_{max}(top)_{sk}$ of the upper skeletal entrance of CDs: (a) **0a**−**3a**; (b) **1b**−**3b**; (c) **0c**−**3c**.

macrocyclic forms would be unfavorable at room temperature. The average trajectory energy of form *a* (**0a**) is lower than that of form *c* (**0c**) by 23.58 kJ/mol ($\Delta\langle E\rangle$**0a**−**0c** = −23.58 kJ/mol, see Tables S14−S15 in the Supporting Information). Note that for structure **0b** the conformation of the $^0S_2$ glucose ring is changed to $^1C_4$ during the equilibration step in the MD simulation, and this conversion process was still observed when constraint to the $^0S_2$ ring was applied to the torsion angles within the ring with a force constant of 500 kJ/mol. The glycosidic O−O−O angles are in the range of ∼126−130° for **0a** and ∼90−160° for **0c**. Therefore, to transform the CD macrocycle from **0a** to **0c** requires significant variation in the macrocyclic conformation. Because this transformation process

dx.doi.org/10.1021/jp207985q | J. Phys. Chem. B 2012, 116, 3477−3489

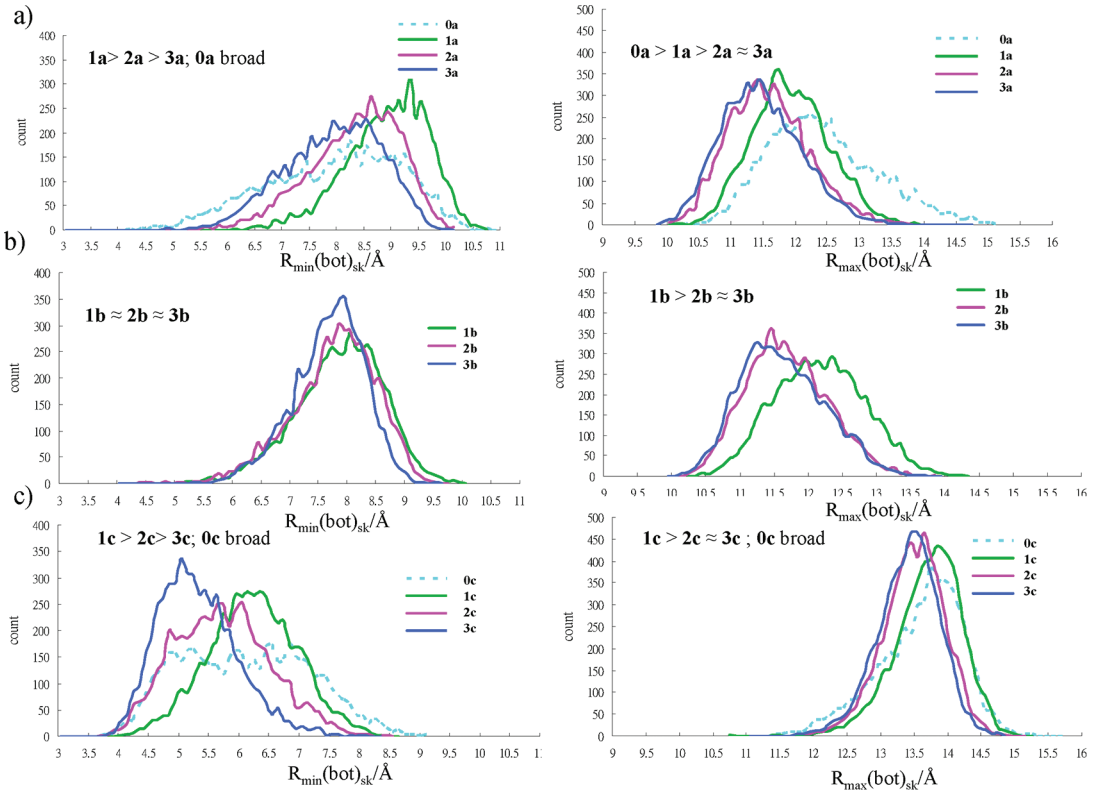

Figure 7. $R_{min}(bot)_{sk}$ and $R_{max}(bot)_{sk}$ of the lower skeletal entrance of CDs: (a) **0a**–**3a**; (b) **1b**–**3b**; (c) **0c**–**3c**.

Table 1. Correlation Coefficients of Various Structural Parameters Calculated from Sampled Structures Obtained from 5000 ps MD Simulations

	$^4C_1$				$^0S_2$			$^1C_4$			
	0a	**1a**	**2a**	**3a**	**1b**	**2b**	**3b**	**0c**	**1c**	**2c**	**3c**
$\Delta R_{l\text{-}s}$ vs $R_{min}(top)_{sk}$	−0.15	−0.34	−0.37	−0.47	−0.45	−0.58	−0.49	−0.58	−0.55	−0.58	−0.53
$\Delta R_{l\text{-}s}$ vs $R_{max}(top)_{sk}$	0.69	0.44	0.54	0.60	0.54	0.54	0.62	0.57	0.71	0.68	0.70
$\Delta R_{l\text{-}s}$ vs $R_{min}(bot)_{sk}$	−0.72	−0.38	−0.53	−0.53	−0.47	−0.44	−0.22	−0.66	−0.49	−0.54	−0.51
$\Delta R_{l\text{-}s}$ vs $R_{max}(bot)_{sk}$	0.55	0.14	0.29	0.24	0.37	0.30	0.35	0.50	0.37	0.20	0.12
$R_{min}(top)_{sk}$ vs $R_{max}(top)_{sk}$	−0.17	−0.30	−0.37	−0.52	−0.15	−0.26	−0.29	−0.35	−0.39	−0.38	−0.40
$R_{min}(bot)_{sk}$ vs $R_{max}(bot)_{sk}$	−0.63	−0.28	−0.46	−0.45	−0.35	−0.31	−0.29	−0.42	−0.25	−0.11	−0.13

Table 2. Correlation Coefficients from Solid State Structures

	0a[a]	**2a**[b]	**3a**[c]
$\Delta R_{l\text{-}s}$ vs $R_{min}(top)_{sk}$	−0.37	−0.36	−0.39
$\Delta R_{l\text{-}s}$ vs $R_{max}(top)_{sk}$	0.66	0.45	0.08
$\Delta R_{l\text{-}s}$ vs $R_{min}(bot)_{sk}$	−0.61	−0.57	−0.48
$\Delta R_{l\text{-}s}$ vs $R_{max}(bot)_{sk}$	0.46	0.25	0.15
$R_{min}(top)_{sk}$ vs $R_{max}(top)_{sk}$	−0.25	−0.88	−0.34
$R_{min}(bot)_{sk}$ vs $R_{max}(bot)_{sk}$	−0.57	−0.48	−0.38

[a]Analyses from 160 β-CD crystal structures with 112 CD dimers and 48 monomers. A total of 225 unique CD monomer structures are measured. [b]Analyses from 16 dimethylated β-CD crystal structures. [c]Analyses from 30 trimethylated β-CD crystal structures; correlation calculated without using structures with $^0S_2$ and $^1C_4$ pyranose rings.

probably requires concerted distortions within the macrocyclic ring, unfavorable activation entropy is expected.

Calculated energy differences between forms *a* and *c* show form *c* of TM-β-CD (**3**) is more easily accessible than their mono- (**1**) and dimethylated (**2**) analogues ($\Delta\langle E\rangle$**3a**−**3c** = −7.97, $\Delta\langle E\rangle$**2a**−**2c** = −27.0, $\Delta\langle E\rangle$**1a**−**1c** = −28.38 kJ/mol; detailed data in Tables S16–S17, Supporting Information). The calculations correlate with the observed behavior in a series of methylated CD structures grown in hot water; only the trimethylated β-CD can be crystallized in form *c*. CD structures in macrocylic form *b*, with a skew-boat $^0S_2$ pyranose ring, have the highest calculated energies for all three methylated CDs ($\Delta\langle E\rangle$**3a**−**3b** = −33.11, $\Delta\langle E\rangle$**2a**−**2b** = −56.14, $\Delta\langle E\rangle$**1a**−**1b** = −47.41 kJ/mol). So far, only the trimethylated β-CD has been observed to adopt the $^0S_2$ form in the TM-β-CD•*m*-iodophenol complex with the presence of guest stabilization. However, the $^0S_2$ macrocycle was observed in the uncomplexed form with bulkier functional groups in the crystal structures heptakis-(2,3,6-tri-*O*-acetyl)-β-CD and heptakis(2,3,6-tri-*O*-propanol)-β-CD.[12]

Electrostatic energy seems to be the determining factor that impedes the mono- and dimethylated β-CDs to adopt the high energy forms *b* and *c*. To convert from *a* to *b* or *c*, the mono- and the dimethyl substituted β-CD have to undergo an electrostatic energy loss of 37.67 (**1a** → **1c**), 45.54 (**1a** → **1b**), 39.16 (**2a** → **2c**), and 44.05 (**2a**→**2b**) kJ/mol (Table S17, Supporting Information, $\Delta\langle E\rangle_{electrostatics}$), whereas, for the trimethylated β-CDs, conversions from **3a** to **3c** and from **3a**

dx.doi.org/10.1021/jp207985q | J. Phys. Chem. B 2012, 116, 3477–3489

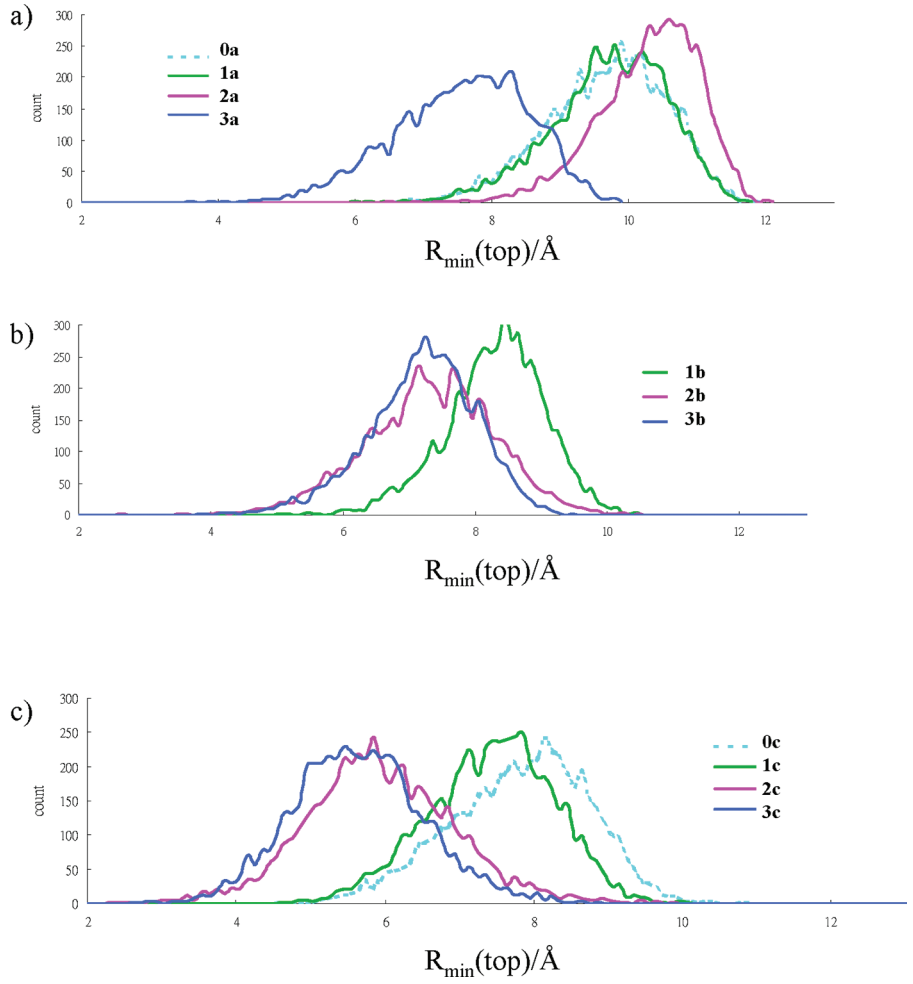

Figure 8. Size of the opening at the top rim of CD structures in (a) **0a**−**3a**, (b) **1b**−**3b**, and (c) **0c**−**3c**.

to **3b** have to incur an electrostatic energy loss of 12.09 and 16.83 kJ/mol, respectively. In the $^4C_1$ chair conformation, O_2, O_3, and C_6 are in the equatorial positions favoring H-bond interactions with adjacent pyranose rings. When the ring is inverted to the skew-boat $^0S_2$ conformation, O_2 and O_3 now occupy the axial positions, and for a full inversion to the $^1C_4$ chair conformation, all three attached atoms occupy axially. Thus, by deforming one of the pyranose rings within the CD, the synchronized H-bonds were disrupted such that O_2 and O_3 on the inverted ring could no longer participate in H-bonding interactions. Because hydrogen bonding is handled as electrostatic interaction in AMBER*, loss of electrostatic energy occurs when the number of hydrogen bonds decreases.

2. Effect of Methylation on the Cavity Shape ($\Delta R_{l\text{-}s}$) of *β*-CD. *β*-CD has a cavity dimension of approximately 6.0−6.5 Å and the height of the torus around 7.9 ± 0.1 Å.[19] Size and shape complementarity between CD and its guest molecule is prerequisite in molecular recognition. The ability of induced fit triggered by guest complexation is inherent in the CD structure, so knowing how the structure of CD fluctuates and how flexible they are, are crucial in controlling molecular recognition in CD complexation. One of the elusive structural characteristics when studying CD complexation is how the cavity shape changes upon complexation with molecular guests varying from bulky three-dimensional to the planar and to the thin chain types of molecules. To monitor the extent to which the cavity shape of *β*-CD and its methylated analogues are varied during MD simulations, $\Delta R_{l\text{-}s}$ is defined (Scheme 3a); it is the calculated difference between the longest and shortest O···O distances from the seven pairs of opposing glycosidic O-atoms in the CD. When $\Delta R_{l\text{-}s}$ is small, it indicates the cavity shape is relatively rounded, whereas an elliptic cavity shape is indicated by a high $\Delta R_{l\text{-}s}$ value.

To understand the structural dynamics of the different CD hosts, we first analyzed the effect of having one of the glucose ring conformations changes from the normal $^4C_1$ form to the $^0S_2$ or $^1C_4$ form in the CD macrocycles. Figure 1a shows the different elliptic distortions of the CD cavities upon changes in one of the glucose conformations. All *c* structures (**0c**−**3c**) have the most elliptic cavity structure ($\Delta R_{l\text{-}s}$ range from 1.3 to 7.2 Å with a mean value of 3.9 Å for **1c**−**3c**; for **0c**, the range is 0.8 to 6.6 Å with a mean value of 3.5 Å). The *b* forms (**1b**−**3b**) are intermediate between *a* and *c* forms ($\Delta R_{l\text{-}s}$ range from 0.3 to 6.2 Å with a mean value of 2.3 Å), and the parent *β*-CD **0a** has a $\Delta R_{l\text{-}s}$ range from 0.1 to 5 Å with a mean value of ca. 1 Å.

For structural type *a*, where all the glucose rings are in the typical $^4C_1$ conformation, the mono- and dimethylated *β*-CDs (**1a** and **2a**) show a very similar $\Delta R_{l\text{-}s}$ trend; *β*-CD **0a** and the permethylated **3a** have a somewhat higher tendency to be elliptic (Figure 1b).[20] In the MD simulations, the percentage of sampled structures with $\Delta R_{l\text{-}s}$ greater than 2 Å for the different CDs are 30, 8, 10, and 15% for **0a**, **1a**, **2a**, and **3a**, respectively. Traditionally, the truncated-cone structure of *β*-CD is considered to be fairly rigid, reinforced by a belt of hydrogen

dx.doi.org/10.1021/jp207985q | J. Phys. Chem. B 2012, 116, 3477−3489

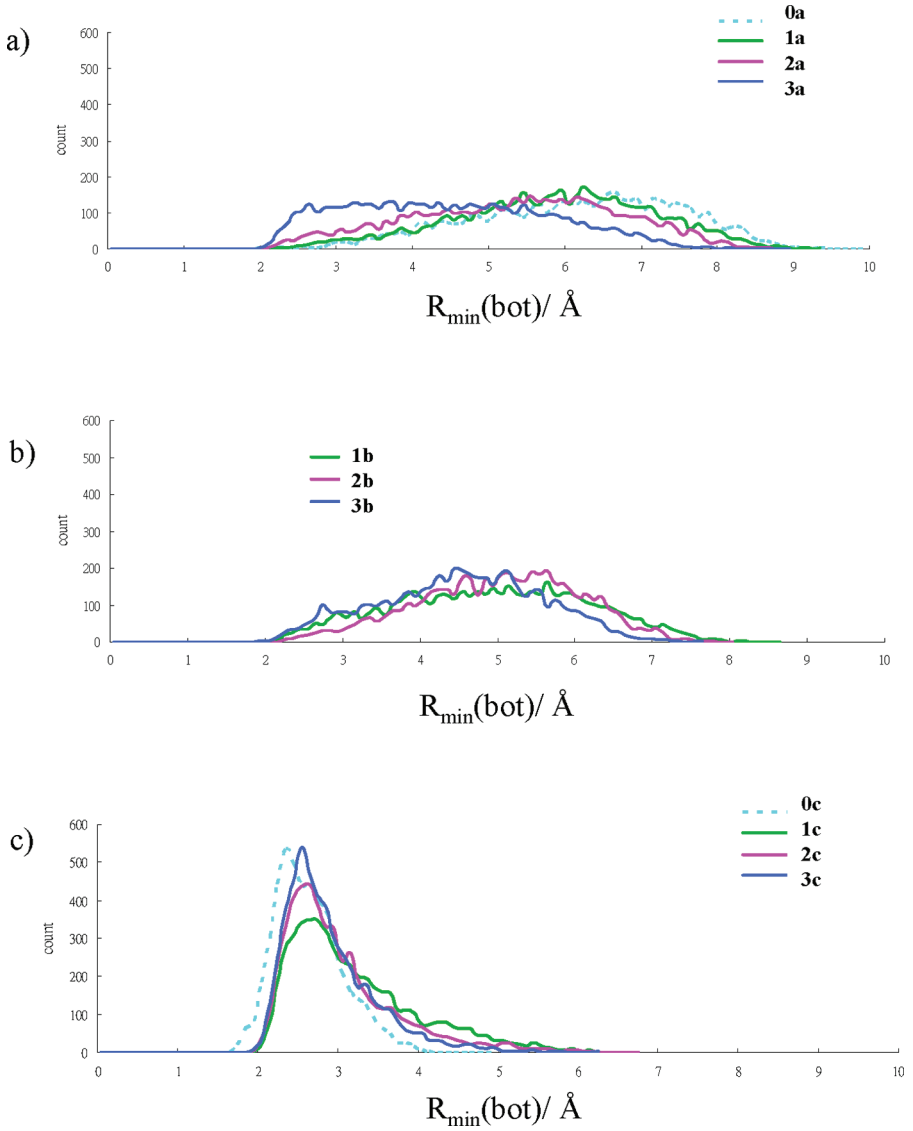

Figure 9. Size of the opening at the bottom rim of CD structures in (a) **0a**–**3a**, (b) **1b**–**3b**, and (c) **0c**–**3c**.

bonding interactions at the top rim of CD. Our simulations showed that the parent β-CD has significant flexibility and as a free host its cavity shape can fluctuate from round to elliptic. For structural type *c*, with one of the glucose rings in the $^1C_4$ configuration, the simulations show that methylation on the unsubstituted **0c** seems to make the cavity more elliptic; there is an obvious shift of $\Delta R_{l\text{-}s}$ values from **0c** to **1c**–**3c** (Figure 1a). The simulations also indicate that further methylation to macrocylic types *b* and *c* (**1b**–**3b** and **1c**–**3c** in Figure 1a) show no significant changes in the cavity shape.

To see how the cavity shape varies in the different crystal structures of CD complexes and how they differ from MD simulation results, $\Delta R_{l\text{-}s}$ was calculated for all the available crystal structures of β-CD and methylated β-CD complexes. To date, only three types of methyl-substituted β-CDs have been structurally characterized: DM-β-CD, TM-β-CD, and an unusual monosubstituted 2-methyl-β-CD.[21] Analyses of X-ray crystal structures for the two common forms, DM- and TM-β-CDs and their inclusion complexes,[5,6] reveal distinct differences in the cavity shape of the CDs. In general, the trimethylated **3a** complexes have a more elliptic CD structure when compared to the dimethylated **2a** complexes (Figure 2a; blue ▲ versus red ◆). The largest $\Delta R_{l\text{-}s}$ values observed for **2a** and **3a** are 0.79 Å (based on 16 structures) and 2.48 Å (30 structures), respectively. Only two available structures of each for **3b** and **3c** conformations have been crystallized, and the largest $\Delta R_{l\text{-}s}$ values are 2.13 and 4.27 Å, respectively (circled in Figure 2). In Figure 2a, $\Delta R_{l\text{-}s}$ is shown according to the type of guest in the CD structures. From the limited number of crystal structures available for evaluation, it seems that **2a** can accommodate guests varying from short chain molecules to the more three-dimensional adamantoid without great distortion of the macrocyclic cavity. For the β-CD complexes,[22] their cavity shows high flexibility with the largest $\Delta R_{l\text{-}s}$ being 2.1 Å. The crystal analyses of **0a** and **3a** complexes revealed that both CD cavities are able to distort their cavities from round to elliptic. Whether **2a** indeed exhibits a more rounded structure is unclear, as the number of available crystal structures is small.

3. Effect on the Tilting of Glucose Rings in CD Macrocycles upon Methylation. The shape and size of the CD cavity is closely related to how each of the glucose rings tilts and the tilted rings can affect the top and bottom entrances of the CD. To analyze the tilting of glucose rings, we define the ring tilt using the angle between the two least-squares mean

dx.doi.org/10.1021/jp207985q | J. Phys. Chem. B 2012, 116, 3477–3489

planes of the glucose ring (defined by atoms C_2, C_3, C_5, and O_5) and the glycosidic mean plane (defined by the seven glycosidic O-atoms). When the two planes are perpendicular, the tilting angle is defined as zero. When O_2 and O_3 (part of the wider top rim) cave in toward the macrocyclic ring center, the tilting angle is defined as positive. With the above definition, the seven chemically equivalent glucose rings of β-CD (**0a**) show overlapping tilt distribution as expected, with a tilting angle range of −70 to 30° and maxima of the distributions centering around −10° (Figure S1, Supporting Information). However, if we renumber the rings relative to the elliptic long axis of the CD cavity for each snapshot structure (see graphical representation in Figure 3, viewing down from the top rim of CD; the long axis is defined by the glycosidic O-atoms), the distributions of ring tilt are no longer equivalent for all rings (Figure 3, **0a**). Some rings tend to tilt out more than others. Therefore, when analyzing a macrocycle which can change from round to elliptic, the above operation of renumbering is important to reveal the true structural features that are difficult to observe otherwise.

Figures 3−5 show the tilting angle population of each glucose ring for the different CD forms *a*−*c*. The population curves are clustered together in Figure 3 (form *a*) but become more and more spread out in Figures 4 and 5 (forms *b* and *c*). Therefore, a clear pattern of increasingly nonequivalent ring tilting behavior is observed as the CD is transformed from form *a* to forms *b* and *c*. Nevertheless, no matter how different the population curves may look among different forms, the two rings next to the elliptic long axis (G4 and G7; in blue in Figures 3−5) tend to tilt out the most, especially G4 in forms *b* and *c*.

Long-range trans-glycosidic scalar spin−spin $^3J_{CH}$ couplings of β-CD measured by NMR and from our simulations are comparable. The couplings related to the ψ (C_1−O_4'−C_4'−H_4') and φ (H_1−C_1−O_4'−C_4') torsion angles, J_ψ and J_φ, are measured to be 5.2 from NMR;[23] from our simulations, they are 6.6 and 6.4, respectively. A recent report showed the calculated J_ψ and J_φ of β-CD to be 6.6 using the CSFF carbohydrate force field.[24] Unmethylated β-CD (**0a**) has a larger tendency to be elliptic than methylated CDs **1a**−**3a** (see last section), and its tilting angle population curves of G4 and G7 of **0a** are noticeably different from that of other rings (Figure 3). MD simulations using a different starting structure, and with a longer simulation time of 20 ns, also show a similar structural feature for **0a** (Figure S2, Supporting Information). Among **1a**−**3a**, the extent of methylation on CD brings minor changes to population of ring tilting.

By transforming one glucose ring configuration within the CD to $^0S_2$, form *b* becomes more elliptic than *a* (see last section). The $^0S_2$ ring resides next to the elliptic long axis and is more tilted in relative to other rings (see G5 in dotted red in Figure 4). The neighboring ring across the long axis has a strong tendency to tilt out (see G4 in dotted blue in Figure 4). These features of form *b* are very different from those of form *a*. Methylation more or less changes the tilting population, but the distinct features of G4 and G5 remain. Similar to the $^0S_2$ ring, the $^1C_4$ glucose ring in **0c**−**3c** is also next to the elliptic long axis (G1 in red in Figure 5). The ring tilts of **0c**−**3c** show the rings are locked into localized regions. In **0c** and **1c**, the ring tilts can be observed to cluster around three distinct regions. Rings with a larger tendency to tilt out or in are drawn in the graphical representation of Figure 5. The rings in **0c** show a broad tilting range but sharpened upon methylation. With the steric effect brought on by the methyl groups in the upper rim of **2c** and **3c**, methylation on *c* makes the rings adopt different tilting regions.

Population analyses of ring tilt show only the distribution of each ring but do not give a direct indication about whether ring tilt and cavity shape are correlated. Therefore, correlation between tilting angle and $\Delta R_{l\text{-}s}$ is carried out for all compounds in different forms (see Tables S18−S20, Supporting Information). The correlation is found to be weak in general. However, the sign of the correlation coefficient indicates a more elliptic cavity could be accompanied by a more significant ring tilt next to the elliptic long axis. For example, the signs for G4 and G5 are negative and positive, respectively. A negative correlation coefficient means a larger $\Delta R_{l\text{-}s}$ value (more elliptic cavity) is prone to have a more negative tilting angle (i.e., tilt-out); a positive value means a more elliptic cavity is prone to have a more tilt-in ring.

4. Effect on the Entrance Size upon Methylation. The wider top rim of CD containing secondary hydroxyl groups is considered to be the main binding site for guest inclusion,[25] but the contribution from the narrower bottom rim should not be overlooked, as demonstrated by the insertion of the carboxylic group at the narrow rim by benzoic acid.[26] As the cavity of CD fluctuates from round to elliptic, the upper and lower rim entrances also exhibit similar behavior. Because the positions of the functional groups attached to $C_2/C_3/C_5$ of a sugar ring determine the size and shape of an entrance, atom-to-atom distances (R values) between every atom of these groups on opposite rings are measured (more details later). It should be noted that, among the atoms of the functional groups, the positions of the $O_2/O_3/C_6$ atoms are determined by the sugar rings and therefore these atoms can be viewed as part of the CD skeleton. On the other hand, the positions of other atoms in the functional group are less so, due to the free rotations around C_2−O_2, C_3−O_3, and C_5−C_6 bonds. Therefore, the R values are analyzed in two ways to reveal the *skeletal* (donated by the subscript "sk") and *actual* rim size (without the subscript). Take the top rim as an example: The skeletal rim size is determined by R values between O_2/O_3 atoms of opposite rings (R_{sk}). For each of the 14 hydroxyl O-atoms on the top rim, a set of three cross-ring distances are measured. In Scheme 3b, it can be seen that, for O_3 in glucose unit 1 (O_{31}), the three measured distances are $O_{31}\cdots O_{34}$, $O_{31}\cdots O_{24}$, and $O_{31}\cdots O_{35}$; for O_2 in glucose 1 (O_{21}), they are $O_{21}\cdots O_{24}$, $O_{21}\cdots O_{35}$, and $O_{21}\cdots O_{25}$. The maximum and minimum of all cross-ring distances thus calculated for each MD snapshot are recorded and termed $R_{max}(top)_{sk}$ and $R_{min}(top)_{sk}$, respectively. For the bottom rim, seven $C_6\cdots C_{6'}$ distances ($C_{61}\cdots C_{64}$, $C_{61}\cdots C_{65}$, $C_{62}\cdots C_{65}$, $C_{62}\cdots C_{66}$, $C_{63}\cdots C_{66}$, $C_{63}\cdots C_{67}$, and $C_{64}\cdots C_{67}$) are measured (see Scheme 3b). The maximum and minimum values are labeled $R_{max}(bot)_{sk}$ and $R_{min}(bot)_{sk}$, respectively. The maximum and minimum values reflect how much the upper/lower rim is opened up due to the expansion of the CD cavity, omitting the crowding effect by the bonded substituent groups on O_2, O_3, and C_6. These values not only show the size of the entrance but also give indication to the shape of the entrance. For an elliptic entrance, a large R_{max} value is accompanied by a smaller R_{min} value (Scheme 3c). Because the actual entrance can be blocked by an inward pointing substituent, cross-ring atom-to-atom distances with the consideration of all of the atoms in the functional groups are also calculated. The minimum R value of each structure is recorded for the upper/lower rim ($R_{min}(top)/R_{min}(bot)$) to

dx.doi.org/10.1021/jp207985q | J. Phys. Chem. B 2012, 116, 3477−3489

show the narrowest part of the entrance. It is noted that R_{max}(top) and R_{max}(bot) are not measured because they are not relevant in determining the entrance size when the functional groups rotate away from the entrances.

i. The Skeletal Rim Size. Population analyses on the entrance dimension for both upper and lower rims of all methylated and non-methylated models are given in Figures 6 and 7. For the non-methylated β-CDs (**0a** and **0c**), changing one of the glucose rings from the $^4C_1$ to $^1C_4$ configuration made the upper and lower skeletal rims more elliptic.[27] That is, both $R_{min}(top)_{sk}$ and $R_{min}(bot)_{sk}$ of **0c** become shorter than **0a**, while $R_{max}(top)_{sk}$ and $R_{max}(bot)_{sk}$ become longer; mean $R_{min}(top)_{sk}$ = 10.30 Å **0a** and 8.75 Å **0c**; mean $R_{min}(bot)_{sk}$ = 8.05 Å **0a** and 6.05 Å **0c**; mean $R_{max}(top)_{sk}$ = 14.15 Å **0a** and 15.0 Å **0c**; mean $R_{max}(bot)_{sk}$ = 12.25 Å **0a** and 13.65 Å **0c**. The same trend is also observed for methylated CDs, as CD changes its configuration from $^4C_1$ (*a*) to $^0S_2$ (*b*) and to $^1C_4$ (*c*) (see Figures 6 and 7). In general, increased methylation on the *a*, *b*, and *c* systems expands the top rim entrance size by lengthening both $R_{min}(top)_{sk}$ and $R_{max}(top)_{sk}$ (TM > DM > Me), and in turn makes the bottom rim smaller ($R_{min}(bot)_{sk}$ and $R_{max}(bot)_{sk}$ are in the order Me > DM > TM). The only exception is for configuration *c* where $R_{min}(top)_{sk}$ shows the trend **0c** > **1c** > **3c** > **2c**, indicating **3c** is generally more elliptic at the upper rim with an even narrower entrance than the parent **0c**.

The expansion of the top skeletal rim is in good agreement with the $O_2\cdots O_{3'}$ distances between adjacent glycose rings monitored during MD. The mean $O_2\cdots O_{3'}$ distances are 3.10 **0a**, 3.02 **1a**, 3.11 **2a**, and 3.34 Å **3a**. As β-CD becomes fully methylated, all the methyl groups bonded on O_3 are pointing toward the cavity, exerting strain in the macrocycle by bumping into the O_2 atoms of adjacent pyranose rings. This forces the skeletal upper rim in **3a** to expand. Analyses of crystal structures of **0a**, **2a**, and **3a** reveal differences from that observed in MD simulations of solvated hosts without specific guest inclusion. In the presence of guest and packing forces in crystal structure, the top skeletal rim of **3a** is much narrower than **0a**, rather than more expanded as observed in MD, with $R_{min}(top)_{sk}$ and $R_{max}(top)_{sk}$ showing the trend **3a** ≪ **0a** ≈ **2a** and **3a** ≫ **0a** ≈ **2a**, respectively (see Figure 2b: $R_{max}(top)_{sk}$ is shown in ● (**0a**), ◆ (**2a**), and ▲ (**3a**); $R_{min}(top)_{sk}$ is shown in ○ (**0a**), ◇ (**2a**), and △ (**3a**)). The same trend is also observed at the bottom skeletal rim (Figure 2c), where **3a** in crystal structures is also narrower than **0a**, **3a** ≪ **0a** for $R_{min}(bot)_{sk}$. In crystal structures of **3a**, an interesting trend is observed for a number of its structures where two glucose rings G2 and G6 on two sides of the long elliptic axis tilt inward. As a consequence, this behavior makes $R_{min}(top)_{sk}$ smaller in **3a**, thus resulting in a narrower top skeletal rim in crystal structures. Crystal structures **3a** also show that G1, G3, G4, and G7 have a preference to tilt out, which plays a role in determining $R_{min}(bot)_{sk}$. Thus, the structural trends observed in the crystalline state **3a** are possibly due to the induced-fit effect to maximize geometric complementarity with the guest molecules. These trends in ring tilting were not found in crystal structures of **0a** and **2a**.

When we compare the calculated correlation coefficients of the various parameters from MD and solid state structures (Tables 1 and 2), the solid state CD structures of **0a**, **2a**, and **3a** show structural correlations consistent with that observed in MD simulations. As the CD cavity gets more elliptic with increasing $\Delta R_{l\text{-}s}$ value, $R_{max}(top)_{sk}$ and $R_{max}(bot)_{sk}$ get longer with a positive correlation value and $R_{min}(top)_{sk}$ and $R_{min}(bot)_{sk}$ get shorter with a negative correlation value. As R_{max} and R_{min} are also negatively correlated, the correlations are consistent with the picture that the rims get more elliptic as the cavity gets more elliptic. We just mentioned above that in crystal structures of **3a** two glucose rings (G2 and G6) tend to tilt inward. This tilting behavior probably causes the cavity ellipticity and top rim $R_{max}(top)_{sk}$ to almost have no correlation, as revealed from the correlation coefficient shown in Table 2 for **3a**.

ii. The Actual Opening at the Upper and Lower Rims. The wider upper rim of CD is considered to be the main binding site for guest complexation. This aperture is controlled by 14 substituent groups that are bonded on the secondary hydroxyl O-atoms. Solid state structures of DM-β-CD **2a** and TM-β-CD **3a** showed methyl groups bonded on O_2 are pointing outward from the CD cavity, while those bonded on O_3 are pointing inward. However, conversion of one pyranose ring to $^0S_2$ and $^1C_4$ makes O_2 point directly toward the CD cavity, and renders its bonded substituent group blocking part of the upper rim entrance. Conversion of CDs from *a* to *b* and then to *c* showed a progressive narrowing of the actual entrance of the upper rim with a general trend of $R_{min}(top)$ *c* < *b* < *a* (Figure 8).

Simulations of structures in *a* form show, as expected, that TM-β-CD **3a** has the narrowest actual top rim opening due to large steric crowding from methylation on all the secondary hydroxyl sites ($R_{min}(top)$ in the range of 4 to 10 Å in Figure 8a). On average, 6-methylated-β-CD **1a** and the parent β-CD **0a** show similar $R_{min}(top)$ values in the range of 6 to 12 Å. A notable observation is that **2a** tends to exhibit a wider top rim opening than **0a** and **1a**. This could be explained by how the methyl groups in **2a** and hydroxyl groups in **1a** or **0a** are orientated within the structures. In **2a**, the bulky methyl groups bonded on O_2 atoms are oriented away from the CD cavity, whereas in **1a** and **0a** the bonded H-atoms on O_2 groups are oriented toward the CD cavity such that they could participate in intramolecular hydrogen bond interactions with adjacent pyranose units, thus giving smaller $R_{min}(top)$ values. A slightly different trend is observed for the CD structures in *b* and *c* forms; **3b** ≈ **2b** < **1b** and **3c** ≈ **2c** < **1c** < **0c** (Figure 8b,c). As discussed earlier, CD structures in *b* and *c* forms have the axial O_2-atoms pointed directly into the cavity in the $^0S_2$ and $^1C_4$ rings, thus resulting in larger steric crowding at the actual top rim in the trimethylated and 2,6-dimethylated β-CDs (**3b**, **3c**, **2b**, and **2c**) than the 6-methylated β-CDs (**1b** and **1c**).

For $R_{min}(bot)$, both *a* and *b* forms show broad distance distributions with the distance range from 2 up to 9 Å (Figure 9). However, structures in *c* form show the narrowest bottom rim opening and much sharper distance distributions ranging from 2 to 7 Å. This means the bottom rim of *c* structures is not as accessible for guest molecules when compared to *a* and *b* structures.

■ CONCLUSION

The main aim of this paper is to offer a simple visualization into how chemical modification of the CD structure affects its conformation. Through demonstration by the study on β-CD and methylated-β-CDs, we show that the defined geometric parameters combining with their corresponding correlation analyses have enabled us to interpret the structural change with greater insights. Overall, the structure correlations observed in our simulations of the solvated free hosts and those from solid state structures do show good agreement. The subtle differences observed, especially in trimethylated-β-CD, can be viewed in terms of the effect imposed by guest inclusion and

dx.doi.org/10.1021/jp207985q | J. Phys. Chem. B 2012, 116, 3477−3489

crystal packing. So far, we have observed how different degrees of methylation have an effect on the overall CD structural features. Changing the configuration of one of the glucose rings within the CD can drastically alter the overall macrocyclic structure, as clearly depicted in $\Delta R_{l\text{-}s}$ and the glucose ring tilts. Within these CD structures, in both MD simulations and crystal structures, our analyses have allowed us to see a coherent relationship between the structural changes of the different CDs and the defined geometric parameters. With the appropriate adaptation of the geometric parameters to other related macrocyclic structures, such as modified α-, β-CDs or even calixarenes, this analysis approach can be a useful tool to gain better insights into their structures.

■ ASSOCIATED CONTENT

Supporting Information

Supporting Tables S1−S20 include calculated energies, correlation coefficients of the different geometric parameters from MD simulations, and correlation coefficients of ring tilts. Figures S1−S4 include analyses from MD simulations. This material is available free of charge via the Internet at http://pubs.acs.org.

■ AUTHOR INFORMATION

Corresponding Author

*E-mail: ichao@chem.sinica.edu.tw. Phone: +886-2-2789-8530. Fax: +886-2-2783-1237.

Notes

The authors declare no competing financial interest.

■ ACKNOWLEDGMENTS

We thank the National Science Council (project number: NSC 97-2113-M-001-018-MY3) for the financial support. We wish to acknowledge the use of the Chemical Database Service at Daresbury. The computing time granted by the National Center for High-Performance Computing and the Computing Center of Academia Sinica is also acknowledged.

■ REFERENCES

(1) (a) Fischer, E. *Ber. Dtsch. Chem. Ges.* **1894**, *27*, 2985−2993. (b) Cram, D. J. *Angew. Chem.* **1986**, *98*, 1041−1060; *Angew. Chem., Int. Ed.* **1986**, *25*, 1039−1057.

(2) Koshland, D. E. Jr. *Proc. Natl. Acad. Sci. U. S. A.* **1958**, *44*, 98−104.

(3) (a) Easson, L. H.; Stedman, E. *Biochem. J.* **1933**, *27*, 1257−1266. (b) Dalgliesh, C. E. *J. Chem. Soc.* **1952**, *3*, 3940−3942. (c) Pirkle, W. H.; Pochapsky, T. C. *Chem. Rev.* **1989**, *89*, 347−362. (d) Kano, K. *J. Phys. Org. Chem.* **1997**, *10*, 286−291.

(4) Inoue, Y. *Annu. Rep. NMR Spectrosc.* **1993**, *27*, 59−101.

(5) (a) Czugler, M.; Eckle, E.; Stezowski, J. *J. Chem. Soc., Chem. Commun.* **1981**, 1291−1922. (b) Aree, T.; Saenger, W.; Leibnitz, P.; Hoier, H. *Carbohydr. Res.* **1999**, *315*, 199−205. (c) Harata, K. *Bull. Chem. Soc. Jpn.* **1988**, *61*, 1939−1944. (d) Aree, T.; Hoier, H.; Schulz, B.; Reck, G..; Saenger, W. *Angew. Chem., Int. Ed.* **2000**, *39*, 897−899. (e) Selkti, M.; Navaza, A.; Villain, F.; Charpin, P.; De Rango, C. *J. Inclusion Phenom. Macrocyclic Chem.* **1997**, *27*, 1−12. (f) Harata, K. *J. Chem. Soc., Chem. Commun.* **1993**, 546−547. (g) Harata, K. *Chem. Commun.* **1999**, 191−192. (h) Steiner, T.; Saenger, W. *Carbohydr. Res.* **1995**, *275*, 73−82. (i) Stezowski, J. J.; Parker, W.; Hilgenkamp, S.; Gdaniec, M. *J. Am. Chem. Soc.* **2001**, *123*, 3919−3926. (j) Aree, T.; Hoier, H.; Reck, G..; Saenger, S. *Angew. Chem., Int. Ed.* **2000**, *39*, 897−899. (k) Tsorteki, F.; Mentzafos, D. *Carbohydr. Res.* **2002**, *337*, 1229−1232.

(6) (a) Harata, K.; Uekama, K.; Otagiri, M.; Hirayama, F. *Bull. Chem. Soc. Jpn.* **1983**, *56*, 1732−1736. (b) Harata, K.; Uekama, K.; Imai, T.; Hirayama, F.; Otagiri, M. *J. Inclusion Phenom. Macrocyclic Chem.* **1988**, *6*, 443−460. (c) Harata, K. *J. Chem. Soc., Chem. Commun.* **1988**, 928−929. (d) Harata, K.; Hirayama, F.; Arima, H.; Uekama, K.; Miyaji, T. *J. Chem. Soc., Perkin Trans. 2* **1992**, 1159−1166. (e) Caira, M. R.; Griffith, V. J.; Nassimbeni, L. R.; van Oudtshoorn, B. *J. Chem. Soc., Perkin Trans. 2* **1994**, 2071−2072. (f) Steiner, T.; Saenger, W. *Angew. Chem., Int. Ed.* **1998**, *37*, 3404−3407. (g) Mentzafos, D.; Mavridis, I. M.; Schenk, H. *Carbohydr. Res.* **1994**, *253*, 39−50. (h) Brown, G. R.; Caira, M. R.; Nassimbeni, L.; van Oudtshoorn, B. *J. Inclusion Phenom. Macrocyclic Chem.* **1996**, *26*, 281−294. (i) Caira, M. R.; Griffith, V. J.; Nassimbeni, L. R.; van Oudtshoorn, B. *J. Inclusion Phenom. Macrocyclic Chem.* **1995**, *20*, 277−290. (j) Makedonopoulou, S.; Yannakopoulou, K.; Mentzafos, D.; Lamzin, V.; Popov, A.; Mavridis, I. M. *Acta Crystallogr.* **2001**, *B57*, 399−409. (k) Rontoyianni, A.; Mavridis, I. M.; Israel, R.; Beurskens, G. *J. Inclusion Phenom. Macrocyclic Chem.* **1998**, *32*, 415−428. (l) Cardinael, P.; Peulon, V.; Perez, G.; Coquerel, G.; Toupet, L. *J. Inclusion Phenom. Macrocyclic Chem.* **2001**, *39*, 159−167.

(7) Immel, S.; Fujita, K.; Lichtenthaler, F. W. *Chem.—Eur. J.* **1999**, *5*, 3185−3192.

(8) Fujita, K.; Chen, W.-H.; Yuan, D.-Q.; Nogami, Y.; Koga, T.; Fujioka, T.; Mihashi, K.; Immel, S.; Lichtenthaler, F. W. *Tetrahedron: Asymmetry* **1999**, *10*, 1689−1696.

(9) (a) Lichtenthaler, F. W.; Immel, S. *Tetrahedron: Asymmetry* **1994**, *5*, 2045−2060. (b) Lindner, H. J.; Yuan, D.-Q.; Fujita, K.; Kubo, K.; Lichtenthaler, F. W. *Chem. Commun.* **2003**, 1730−1731.

(10) (a) Kida, T.; Michinobu, T.; Zhang, W.; Nakatsuji, Y.; Ikeda, I. *Chem. Commun.* **2002**, 1596−1597. (b) Morales, J. C.; Zurita, D.; Penadés, S. *J. Org. Chem.* **1998**, *63*, 9212−9222. (c) Hoffmann, B.; Bernet, B.; Vasella, A. *Helv. Chim. Acta* **2002**, *85*, 265−287. (d) Bodine, K. D.; Gin, D. Y.; Gin, M. S. *J. Am. Chem. Soc.* **2004**, *126*, 1638−1639. (e) Kikuzawa, A.; Kida, T.; Akashi, M. *Org. Lett.* **2007**, *9*, 3909−3912. (f) Li, W.-W.; Claridge, T. D.W.; Li, Q.; Wormald, M. R.; Davis, B. G.; Bayley, H. *J. Am. Chem. Soc.* **2011**, *133*, 1987−2001. (g) Bornaghi, L.; Utille, J.-P.; Penninga, D.; Schmidt, A. K.; Dijkhuizen, L.; Schulz, G. E.; Driguez, H. *Chem. Commun.* **1996**, 2541−2542. (h) Kikuzawa, A.; Kida, T.; Nakatsuji, Y.; Akashi, M. *J. Org. Chem.* **2005**, *70*, 1253−1261.

(11) Reibenspies, J. H.; Maynard, D. K.; Derecskei-Kovacs, A.; Vigh, G. *Carbohydr. Res.* **2000**, *328*, 217−227.

(12) Añibarro, M.; Gessler, K.; Usón, I.; Sheldrick, G. M.; Harata, K.; Uekama, K.; Hirayama, F.; Abe, Y.; Saenger, W. *J. Am. Chem. Soc.* **2001**, *123*, 11854−11862.

(13) MacroModel, Interactive Molecular Modeling System, Version 6.5, BatchMin, Columbia University, NY. MacroModel Version 9.0, Schrodinger, LLC, New York, NY, 2011.

(14) (a) Weiner, S. J.; Kollman, P. A.; Case, D. A.; Singh, U. C.; Chio, C.; Alagona, G.; Profeta, S.; Weiner, P. *J. Am. Chem. Soc.* **1984**, *106*, 765−784. (b) Weiner, S. J.; Kollman, P. A.; Case, D. A. *J. Comput. Chem.* **1986**, *7*, 230−252.

(15) (a) Still, W. C.; Tempczyk, A.; Hawley, R. C.; Hendrickson, T. *J. Am. Chem. Soc.* **1990**, *112*, 6127−6129. (b) Qiu, D.; Shenkin, P. S.; Hollinger, F. P.; Still, W. C. *J. Phys. Chem. A* **1997**, *101*, 3005−3014. (c) Weiser, J.; Weiser, A. A.; Shenkin, P. S.; Still, W. C. *J. Comput. Chem.* **1998**, *19*, 797−808. (d) Weiser, J.; Weiser, A. A.; Shenkin, P. S.; Still, W. C. *J. Comput. Chem.* **1998**, *19*, 1110.

(16) During the actual 5000 ps averaging stage for all simulations, small energy and temperature spans (less than 6 kJ/mol and 1.5 K) were found.

(17) Stigler, S. M. Francis Galton's Account of the invention of Correlation. *Stat. Sci.* **1989**, *4* (2), 73−79.

(18) Cloran, F.; Carmichael, I.; Serianni, A. S. *J. Am. Chem. Soc.* **1999**, *121*, 9843−9851.

(19) Szejtli, J. *Chem. Rev.* **1998**, *98*, 1743−1753.

(20) MD simulations carried out for 20 ns for **0a**−**3a** show the same trend (see Figure S3, Supporting Information). In addition, MD simulations of **0a** carried out using two different starting CD structures show similar $\Delta R_{l\text{-}s}$ values (see Figure S4, Supporting Information).

(21) Reibenspies, J. H.; Maynard, D. K.; Derecskei-Kovacs, A.; Vigh, G. *Carbohydr. Res.* **2000**, *328*, 217−227.
(22) Analyses of 160 crystal structures with 112 CD dimers and 48 monomers were obtained from The Cambridge Crystallographic Data Centre. http://www.ccdc.cam.ac.uk (accessed March, 2011). New software for searching the Cambridge Structural Database and visualising crystal structures. Bruno, I. J.; Cole, J. C.; Edgington, P. R.; Kessler, M.; Macrae, C. F.; McCabe, P.; Pearson, J.; Taylor, R. *Acta Crystallogr.* **2002**, *B58*, 389−397.
(23) Thaning, J.; Stevensson, B.; Ostervall, J.; Naidoo, K. J.; Widmalm, G.; Maliniak, A. *J. Phys. Chem. B* **2008**, *112*, 8434−8436.
(24) Naidoo, K. J.; Gamieldien, M. R.; Chen, J. Y.-J.; Widmalm, G.; Maliniak, A. *J. Phys. Chem. B* **2008**, *112*, 15151−15157.
(25) Schneider, H.-J.; Hacket, F.; Rudiger, V. *Chem. Rev.* **1998**, *98*, 1755−1784.
(26) Gelb, R. I.; Schartz, L. M.; Johnson, R. F.; Laufer, D. A. *J. Am. Chem. Soc.* **1978**, *100*, 3553−3559.
(27) The $^{0}S_{2}$ pyranose ring of **0b** was converted to a $^{4}C_{1}$ ring during the equilibration step, and this happened even when constraints were applied. Thus, **0b** is not used in the discussion.